JOURNAL OF THEORETICAL AND APPLIED MECHANICS
62, 1, pp. 157-169, Warsaw 2024
https://doi.org/10.15632/jtam-pl/177173

ANALYSIS AND CALCULATION OF STRESS INTENSITY FACTORS FOR TYPE I CRACKS ON THE EDGE OF ELLIPTICAL HOLES UNDER INTERNAL PRESSURE

Shiwei Chen
College of Energy and Mining Engineering, Shandong University of Science and Technology, Qingdao, China
Minglu Xing
State Key Laboratory of Mining Disaster Prevention and Control Co-founded by Shandong Province and the Ministry of Science and Technology, Shandong University of Science and Technology, Qingdao, China, and
College of Energy and Mining Engineering, Shandong University of Science and Technology, Qingdao, China
Yaxin Liu
College of Energy and Mining Engineering, Shandong University of Science and Technology, Qingdao, China
e-mail: liuyaxinlyx0309@163.com
Yanchun Yin, Yurong Li
State Key Laboratory of Mining Disaster Prevention and Control Co-founded by Shandong Province and the Ministry of Science and Technology, Shandong University of Science and Technology, Qingdao, China, and
College of Energy and Mining Engineering, Shandong University of Science and Technology, Qingdao, China
Longfei Li
College of Energy and Mining Engineering, Shandong University of Science and Technology, Qingdao, China

The stress intensity factor and stress field expression for long cracks near an infinite-length plate bore are calculated using the Muskhelishvili Complex Function Approach. It applies to engineered bore edge cracks, especially under the condition in which the elliptical bore is subjected to internal pressure or only the surface of the crack is subjected to internal pressure. The formula is validated by numerical simulation and applies both to elliptical and circular holes. The variation of stress intensity factor with crack length is analyzed when the special round hole is only subjected to internal pressure. It has practical application value in fracture engineering.

Keywords: Muskhelishvili complex function, stress intensity factor, single elliptical fissure hole, numerical simulation

1. Introduction

In recent years, rock fragmentation by expansion is a common method of rock fragmentation in tunnel engineering (Guo *et al.*, 2017). It does not only cause rock fragmentation in a short period of time, but also allows secondary rock disintegration. Its economic advantages of environmental protection, efficiency and applicability have been widely recognized in engineering. During the formation period and excavation disturbance, a large number of cracks is generated in the rock mass, and the existence of cracks reduces mechanical strength and deformation resistance of the rock mass (Zhang *et al.*, 2022, 2023a). Hole-edge cracks are a commonly observed type of cracks in engineering structures. However, due to their discontinuous nature at the interface, analytical solutions are difficult to obtain directly. Fracture mechanics has made significant progress in both theoretical and numerical approaches over the years (Zhang *et al.*, 2023b; Alderliesten, 2007; Fett, 1992; Aliabadi *et al.*, 1987; Parker and Andrasic, 1983; Andrasic and Parker, 1984;

Bakuckas, 2001; Brennan and Ten, 2004; Chen *et al.*, 2001; Deng and Matsumoto, 2017). Bowie (1956, 1964) employed numerical techniques to compute the stress intensity factors of single--hole single-crack or single-hole double-crack configurations in an infinite flat plate subjected to uniaxial or biaxial loading.

Xu *et al.* (2018) employed a weight function closure method to address the opening displacement of a symmetrical double crack with a circular hole in an infinite flat plate under partial stress on the crack surface. They provided a crack surface displacement equation for partial cracks under uniform stress through fitting calculation results from the weight function method. Hasebe and Chen (1996) investigated the analytical solution of a single crack defect on the edge of a circular hole, assuming that the crack surface receives uniform internal pressure and the edge of the hole is free, using complex variable function methods and function theory methods. They provided an expression for the stress intensity factor. Zhao *et al.* (2012) utilized a complex function method, constructing a transcendental function to map a single crack on the edge of an elliptical hole onto a complex plane, and provided an expression for the stress intensity factor. Gao *et al.* (2003a,b) were the first to apply the Stroh formula to solve the exact problem of elliptical holes containing a single and two collinear permeable cracks in magnetoelectric elastomers, and their research results could serve as a benchmark for testing the effectiveness of analytical methods for solving more complex crack problems. Xu and Yang (2022) solved the anti-plane fracture problem of regular hexagonal hole edge cracks in composite materials using complex variable function methods and studied their crack propagation laws. Zhu *et al.* (2016) and Yan (2007) investigated the stress intensity factor and opening displacement of double cracks at the edge of an infinite flat plate under stress.

The above research results are all aimed at geometric forms of single or collinear cracks along the edge of the hole. Zhou *et al.* (2020) also used the finite-cut weight function method to solve the crack problem at the edge of the hole. However, for a single crack on the edge of an elliptical hole, there are two types of weight functions: analytical and numerical. Nonetheless, the accuracy of the horizontal weight functions derived from diverse analytical techniques considerably varies, necessitating stringent verification. As of now, there is currently limited literature on the exact analytical solution of a single crack problem on the edge of an elliptical hole.

This paper employs the Muskhelishvili Complex Function method and Cauchy integral theory along with the superposition principle of elasticity to calculate the stress intensity factor. Specifically, the stress intensity factor is calculated under the condition that only the circular hole is subject to a uniform force and the crack surface is not under stress. The Abaqus cloud image fusion method is used to solve and verify the stress intensity factor, which serves as a basis for predicting the fatigue growth life of the crack near the elliptical hole on an infinite plate.

2. Muskhelishvili complex function method

Assuming the presence of an ellipse in an isotropic infinite plane with a crack located on the edge of its hole, the surface of the hole is subjected to uniform internal pressure, while there is no force at infinity, as shown in Fig. 1.

The governing equation for this problem is

$$\nabla^2\nabla^2 U = 0 \tag{2.1}$$

where $\nabla^2 = \partial^2/\partial x^2 + \partial^2/\partial y^2$, U represents the Airy stress function, and

$$\sigma_{yy} = \frac{\partial^2 U}{\partial x^2} \qquad \sigma_{xx} = \frac{\partial^2 U}{\partial y^2} \qquad \sigma_{xy} = -\frac{\partial^2 U}{\partial x \partial y} \tag{2.2}$$

where σ_{ij} is the stress component.

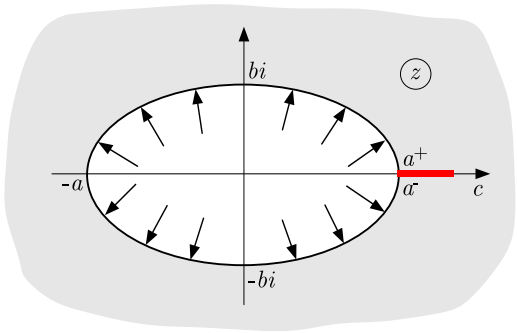

Fig. 1. Force diagram of an elliptical hole

According to literature (Bowie, 1964)

$$U(x,y) = \operatorname{Re}\left[\overline{z}\varphi_1(z) + \int \psi_1(z)\,dz\right] \tag{2.3}$$

where $\varphi_1(z)$ and $\psi_1(z)$ are two analytical functions representing the complex variable $z = x + \mathrm{i}y$, $\overline{z}$ is the conjugate of z; Re represents the real part of a complex number.

From the basic relationship of static elasticity and Eq. (2.3), the expressions for stress and displacement can be obtained as

$$\begin{aligned}
&\sigma_{xx} + \sigma_{yy} = 2[\varphi_1' + \overline{\varphi_1'(z)}] = 4\operatorname{Re}\varphi_1'(z)\\
&\sigma_{yy} - \sigma_{xx} + \mathrm{i}\sigma_{xy} = 2[\overline{z\varphi_1''(z)} + \psi_1'(z)]\\
&2\mu(u_x + \mathrm{i}u_y) = \kappa\varphi_1(z) - \overline{z\varphi(z)} - \overline{z\varphi_1'(z)} - \overline{\psi_1(z)}
\end{aligned} \tag{2.4}$$

where $\kappa = (3-v)/(1+v)$ represents the plane stress state, $\kappa = 3 - 4v$ represents the plane strain state.

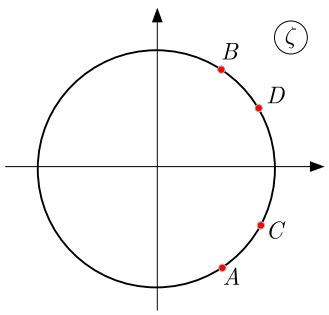

Fig. 2. Mapping from the elliptical to circular hole

If a suitable conformal mapping $z = \omega(\zeta)$ can be mapped, i.e. mapping the region on the physical plane z to the interior of the unit circle on the ζ plane (as shown in Fig. 2, then equations (2.1), (2.2) and (2.3) become

$$\begin{aligned}
&\sigma_\theta + \sigma_\rho = 4\operatorname{Re}\varphi(z)\\
&\sigma_\theta - \sigma_\rho - 2\mathrm{i}\tau_{\rho\theta} = \frac{2\zeta^2}{\rho^2\overline{\omega}'(\zeta)}[\overline{\omega}(\zeta)\phi'(\zeta) + \omega'(\zeta)\psi(\zeta)]\\
&\frac{E}{1+\mu}(u_\rho + \mathrm{i}u_\theta) = \frac{\overline{\zeta}}{\rho}\frac{\overline{\omega}'(\zeta)}{|\omega'(\zeta)|}\Big[\frac{3-\mu}{1+\mu}\varphi(\zeta) - \frac{\omega(\zeta)}{\overline{\omega}(\zeta)}\overline{\varphi}'(\zeta) - \overline{\psi}'(\zeta)\Big]
\end{aligned} \tag{2.5}$$

Among them, (ρ,θ) is ζ the polar coordinate of a plane, with

$$\begin{aligned}&\varphi_1(z)=\varphi_1[\omega(\zeta)]=\varphi(\zeta) \qquad \psi_1(z)=\psi_1[\omega(\zeta)]=\psi(z)\\&\varphi_1'(z)=\frac{\varphi'(\zeta)}{\omega'(\zeta)}=\phi(\zeta) \qquad \psi_1'(z)=\frac{\psi'(\zeta)}{\omega'(\zeta)}=\psi(\zeta)\end{aligned} \tag{2.6}$$

For the unknown functions $\varphi(\zeta)$ and $\psi(\zeta)$, the following functional equations (Fett, 1992) are satisfied

$$\begin{aligned}&\varphi(\zeta)=\frac{1+\mu}{8\pi}(f_x+\mathrm{i}f_y)\ln\zeta+B\omega(\zeta)+\varphi_0(\zeta)\\&\psi(\zeta)=-\frac{3-\mu}{8\pi}(f_x-\mathrm{i}f_y)\ln\zeta+(B'+\mathrm{i}C')\omega(\zeta)+\psi_0(\zeta)\end{aligned} \tag{2.7}$$

where f_x and f_y represent boundary conditions within the plane region, and B and $B'+\mathrm{i}C'$ represent boundary conditions at infinity, which are

$$B=\frac{1}{4}(\sigma_1+\sigma_2) \qquad B'+\mathrm{i}C'=-\frac{1}{2}(\sigma_1-\sigma_2)\mathrm{e}^{-2\mathrm{i}\alpha} \tag{2.8}$$

where α denotes the angle between the principal stress σ_1 at infinity and the Ox axis.

In equations (2.7), $\varphi_0(\zeta)$ and $\psi_0(\zeta)$, respectively

$$\begin{aligned}&\varphi_0(\zeta)+\frac{1}{2\pi\mathrm{i}}\int\limits_\sigma\frac{\overline{\omega(\sigma)}}{\omega'(\sigma)}\frac{\overline{\varphi_0'(\sigma)}}{\sigma-\zeta}\,d\sigma=\frac{1}{2\pi\mathrm{i}}\int\limits_\sigma\frac{f_0}{sigma-\zeta}\,d\sigma\\&\psi_0(\zeta)+\frac{1}{2\pi\mathrm{i}}\int\limits_\sigma\frac{\overline{\omega(\sigma)}}{\omega'(\sigma)}\frac{\overline{\varphi_0'(\sigma)}}{\sigma-\zeta}\,d\sigma=\frac{1}{2\pi\mathrm{i}}\int\limits_\sigma\frac{\overline{f}_0}{\sigma-\zeta}\,d\sigma\end{aligned} \tag{2.9}$$

where

$$f_0=\mathrm{i}\int(\overline{f}_x+\mathrm{i}\overline{f}_y)\,ds-\frac{f_x+\mathrm{i}f_y}{2\pi}\ln\sigma-\frac{1+\mu}{8\pi}(f_x-\mathrm{i}f_y)\frac{\omega(\sigma)}{\overline{\omega'(\sigma)}}-2B\omega(\sigma)-(B'-\mathrm{i}C')\overline{\omega}(\sigma) \tag{2.10}$$

Perform conformal mapping as follows (Deng and Matsumoto, 2017)

$$z=\omega(\zeta)=\frac{a+b}{2}\frac{1+\sqrt{\left(\frac{1+\zeta}{1-\zeta}\right)^2+k^2}}{1-\sqrt{\left(\frac{1+\zeta}{1-\zeta}\right)^2+k^2}}+\frac{a-b}{2}\frac{1-\sqrt{\left(\frac{1+\zeta}{1-\zeta}\right)^2+k^2}}{1+\sqrt{\left(\frac{1+\zeta}{1-\zeta}\right)^2+k^2}} \tag{2.11}$$

where

$$c+a=\alpha \qquad c-a=\beta \qquad k=\frac{\beta-b+\sqrt{\alpha\beta+b^2}}{\alpha+b+\sqrt{\alpha\beta+b^2}}$$

This mapping maps an infinite flat plate with a single cracked elliptical hole on the physical plane shown in Fig. 1 to the interior of the unit circle on the mathematical plane shown in Fig. 2, and has

$$\begin{aligned}&\omega^{-1}(-a)\to-1 \qquad \omega^{-1}(c)\to 1\\&\omega^{-1}(-bi)\to A \qquad \omega^{-1}(bi)\to B\end{aligned} \tag{2.12}$$

Thus, equations (2.9) can be solved under various boundary conditions.

After determining the function $\varphi(\zeta)$, one can obtain a very important physical quantity in fracture theory – the stress intensity factor.

The introduction of the complex stress intensity factor (Alderliesten, 2007) is

$$K_I^{(c,0)} - \mathrm{i}K_{II}^{(c,0)} = 2\sqrt{\pi}\lim_{\zeta\to 1}\sqrt{|\omega(\zeta)-c|}\frac{\varphi'(\zeta)}{\sqrt{\omega'(1)}} = 2\sqrt{\pi}\lim_{\zeta\to 1}\frac{\varphi'(\zeta)}{\sqrt{\omega''(1)}} \tag{2.13}$$

From here, it can be seen that as long as $\varphi'(\zeta)$ is determined, K_I and K_{II} can be obtained.

The following calculations are based on the specific boundary conditions of the problem. From equation (2.11), when $|\sigma| = 1$, $\omega(1/\sigma) = \omega(\sigma)$ can be obtained, where

$$H(\infty) = \frac{1}{2\pi\mathrm{i}}\int\limits_{\gamma}\frac{\omega(\sigma)}{\omega\left(\frac{1}{\sigma}\right)'}\varphi_0'\Big(\frac{1}{\sigma}\Big) \tag{2.14}$$

Then $H(\zeta)$ is analyzed outside the unit circle and can be extended to a continuous function on the circumference. It can be concluded that

$$\frac{1}{2\pi\mathrm{i}}\int\limits_{\gamma}\frac{\omega(\sigma)}{\omega\left(\frac{1}{\sigma}\right)'}\varphi_0'\Big(\frac{1}{\sigma}\Big) = H(\infty) = 0 \tag{2.15}$$

As shown in Fig. 3, first consider an infinite plate under uniform pressure at both elliptical and crack edges, with a pressure of q. In this case

$$f_0(\sigma) = -qz = -q\omega(\sigma) \qquad \varphi(\zeta) = \frac{q}{2\pi\mathrm{i}}\int\limits_{\gamma}\omega(\sigma)\frac{1}{\sigma-\zeta}\,d\sigma \tag{2.16}$$

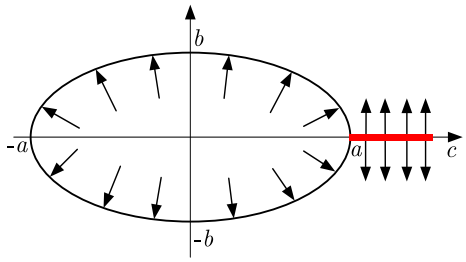

Fig. 3. Stress diagram of the ellipse with cracks

Due to the fact that there is no force on the boundary of the flat plate at infinity, and the forces on the elliptical hole and crack are balanced, the following holds

$$f_x = f_y = B = B' = C' = 0 \tag{2.17}$$

From equations $(2.7)_1$ and (2.11), it can be concluded that from equations $(2.7)_1$ and (2.11), one arrives at

$$\begin{aligned}\varphi_0'(\zeta) = \varphi'(\zeta) &= -\frac{p}{2\pi\mathrm{i}}\int\limits_{\gamma}\frac{\omega'(\sigma)}{\sigma-\zeta}\,d\sigma = \frac{a+b}{4}(g+1)\\ \lim_{\zeta\to 1}\frac{1}{\sqrt{\omega''(1)}} &= \frac{\sqrt{2(g^2-1)}}{\sqrt{(g+1)\Big[a(g^2-1)+bg\sqrt{g^2-1}\Big]}}\end{aligned} \tag{2.18}$$

where

$$g = \frac{(a+b)^2 + \Big(c+\sqrt{\alpha\beta+b^2}\Big)^2}{2(a+b)\Big(c+\sqrt{\alpha\beta+b^2}\Big)}$$

Replace Eqs. (2.9) with Eq. (2.14), and note that when both the hole and crack are subjected to uniform internal pressure, $K_{II}(c,0)=0$, there is

$$K_I'(c,0)=2\sqrt{\pi}\lim_{\zeta\to 1}\frac{\varphi_0'}{\sqrt{\omega''(1)}}=\frac{(a+b)p\sqrt{\pi(g+1)(g^2-1)}}{\sqrt{2\Big[a(g^2-1)+bg\sqrt{g^2-1}\Big]}} \tag{2.19}$$

for the case where only the crack surface is under pressure and the pore surface is not under force, as shown in Fig. 4. Their the elliptical hole edge crack is mapped to the mathematical plane through equation $(2.5)_3$. ζ is inside the unit circle above, and the lower bank a^- of the crack initiation point a is mapped to point C, and the upper bank a^+ of a is mapped to point D.

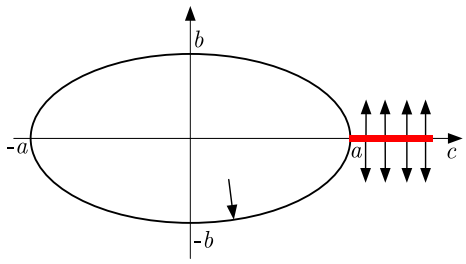

Fig. 4. Crack stress diagram only

On the arc segment of a^+ from the lower bank z_1 of a to the upper bank a^- counterclockwise, $f_1=-qz=-q\omega(\zeta)$, and on the arc segment of a^+ from the upper bank z_2 of a to the lower bank z_1 counterclockwise, $f_1=-qz_2$. The combined surface force acting on the crack at the edge of the hole is 0, and there is no force at infinity. According to equation $(2.18)_1$, it can be obtained

$$\varphi_{oL}(\zeta)=\frac{q}{2\pi\mathrm{i}}\int\limits_{AB}\omega(\sigma)\frac{1}{\sigma-\zeta}\,d\sigma+\frac{qz_2}{2\pi\mathrm{i}}\int\limits_{BA}\frac{1}{\sigma-\zeta}\,d\sigma \tag{2.20}$$

Similarly, according to Eq. (2.14), the stress intensity factor under uniform internal pressure can only be obtained on the crack surface

$$K_{I(OL)}^{(c,0)}=2\sqrt{\pi}\lim_{\zeta\to 1}\frac{\sqrt{2(g^2-1)}\frac{q}{2\pi\mathrm{i}}\int\limits_{AB}\frac{\omega(\sigma)'}{\sigma-\zeta}\,d\sigma}{\sqrt{(g+1)\Big[a(g^2-1)+bg\sqrt{g^2-1}\Big]}} \tag{2.21}$$

Using the superposition principle of elastic fracture mechanics (Alderliesten, 2007), subtract the crack stress intensity factor in Fig. 3 and the crack stress intensity factor in Fig. 4 to obtain the expression of the stress intensity factor in Fig. 1

$$K_{I(O)}^{(c,0)}=K_I^{(c,0)}-K_{I(OL)}^{(c,0)} \tag{2.22}$$

Substitute Eqs. (2.19) and (2.21) into Eq. (2.22) to obtain the stress intensity factor of the crack at the edge of an elliptical hole in an infinite flat plate under stress

$$K_{I(O)}^{(c,0)}=\frac{q\sqrt{\pi(g^2-1)}\Big[\alpha\sqrt{g+1}-\frac{q}{2\pi\mathrm{i}}\int\limits_{\gamma 12}\frac{\omega(\sigma)}{\sigma-\zeta}\,d\sigma\Big]}{\sqrt{2\Big[a(g^2-1)+bg\sqrt{g^2-1}\Big]}} \tag{2.23}$$

It is worth noting that when ζ is on the integration path, equation (2.14) is a singular integral equation, and the approximate calculation of the Cauchy principal value integral needs to be

considered. In this paper, singular point separation and a finite difference numerical method are used for calculation.

In order to clearly express the stress distribution near the crack tip, a polar coordinate system with the crack endpoint as the origin (commonly referred to as the crack leading edge coordinate system) $\zeta = re^{i\theta} = c + \zeta$ is introduced, so $z^2 - a^2 = (z + a)(z - a) = (2a + \zeta)\zeta$.

In the region near the crack end, $|\zeta| = r \ll 2a$, using the binomial theorem, expand the complex variable function of stress at the crack end within the convergence range of $|\zeta| < a$, to obtain

$$\begin{aligned}
\sigma_x &= \frac{K_I}{\sqrt{2\pi r}} \cos\frac{\theta}{2}\left(1 - \sin\frac{\theta}{2}\sin\frac{3\theta}{2}\right) + o(r^{-1/2}) \\
\sigma_y &= \frac{K_I}{\sqrt{2\pi r}} \cos\frac{\theta}{2}\left(1 + \sin\frac{\theta}{2}\sin\frac{3\theta}{2}\right) + o(r^{-1/2}) \\
\tau_{xy} &= \frac{K_I}{\sqrt{2\pi r}} \sin\frac{\theta}{2}\cos\frac{\theta}{2}\cos\frac{3\theta}{2}
\end{aligned} \tag{2.24}$$

3. Numerical calculation analysis

3.1. Calculation model

In order to verify the correctness of the analytical solution for the I stress intensity factor at the crack tip, a planar model was established using Abaqus to simulate and calculate the elliptical hole model with a single crack.

Considering that the plane model is an infinitely large flat plate, the size of the flat plate model differs significantly from the proportion of circular holes contained in the modeling process, far exceeding 100 times. Figure 5 shows the calculation model when $a = 4$, $b = 2$ and $c = 1$, with thick red lines indicating pre-fabricated cracks. The mesh type consists of tetrahedral elements, which is densely divided in the vicinity of circular holes and cracks. The boundary conditions of the model are completely fixed around the edges, while the edges of the elliptical hole are subjected to uniform internal pressure, and the cracks are not subjected to pressure. The concentric circle at the crack tip is the integral region of the cloud image.

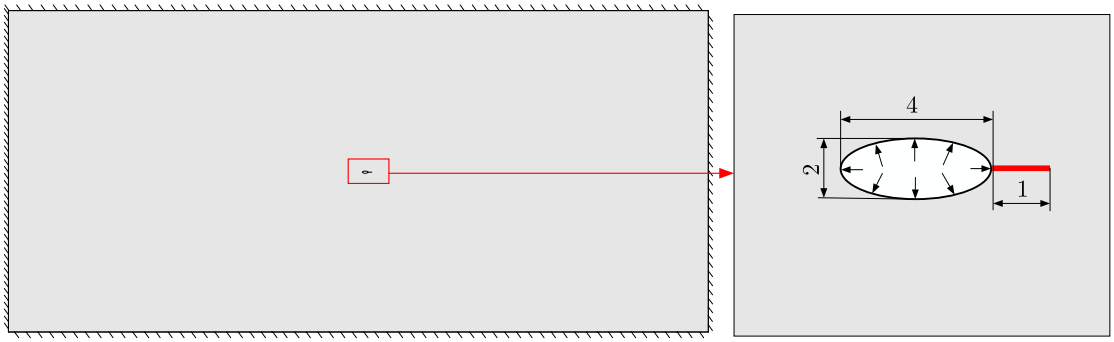

Fig. 5. Crack model, boundary conditions and a stress diagram

In order to reduce the influence of elliptical hole deformation on the calculation of stress intensity factors at the crack tip after loading, the material model of the flat plate is an elastic model, with an elastic modulus of 200 GPa and a Poisson's ratio of 0.25.

3.2. Analysis of the stress field at the crack tip of an elliptical hole

When $a = 4$, $b = 2$, $\beta = 1$, Fig. 6 shows the von Mises stress cloud map and an enlarged grid map of the crack tip finite element model calculated by the Abaqus numerical model.

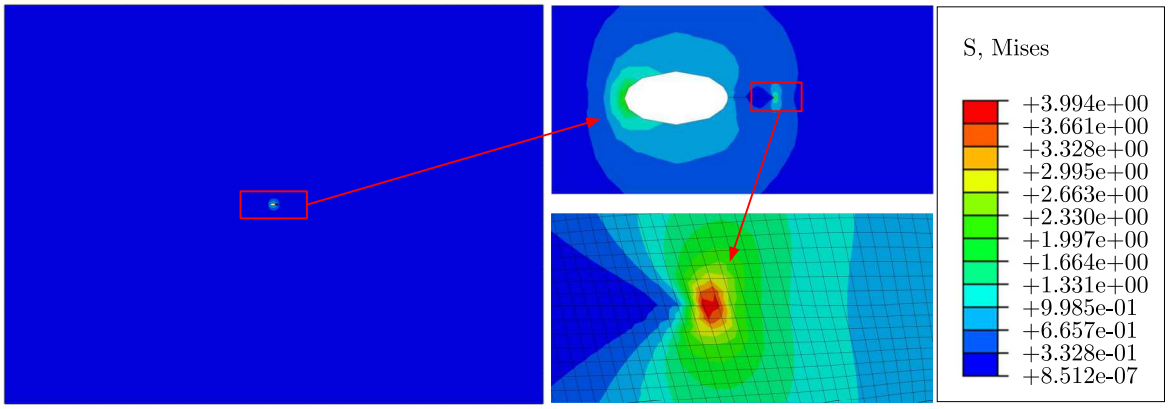

Fig. 6. Crack model and an enlarged stress cloud map of the endpoints

To more intuitively display the distribution law of the stress field at the crack tip of an elliptical hole, adjust the maximum stress values in each direction to be consistent with the von Mises stress, and then draw them separately σ_{xx}, σ_{yy} and τ_{xy}. The stress cloud diagram of τ_{xy} is shown in Figs. 7-9. From the figure, it can be seen that after the elliptical hole is loaded, the stress concentration area appears near the crack tip, and the stress cloud contour lines shown in Figs. 7-9 are consistent with equation (2.24), which is in agreement with the crack tip stress field shown in reference (Li *et al.*, 2010).

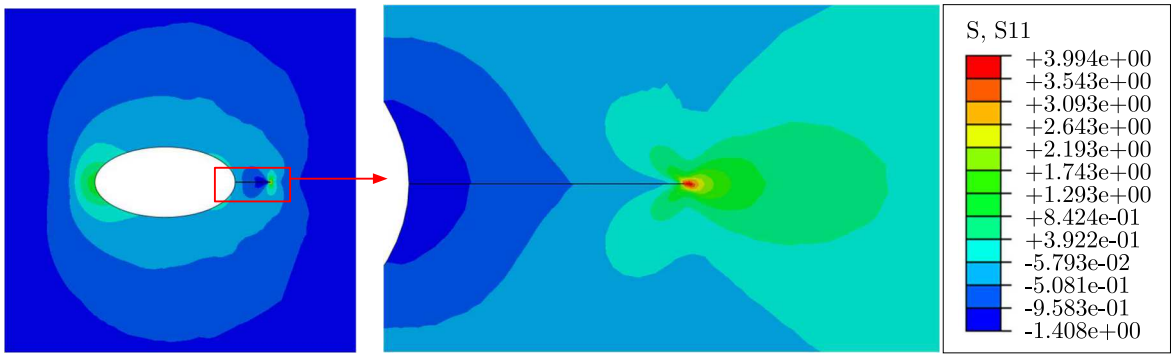

Fig. 7. σ_{xx} force cloud diagram

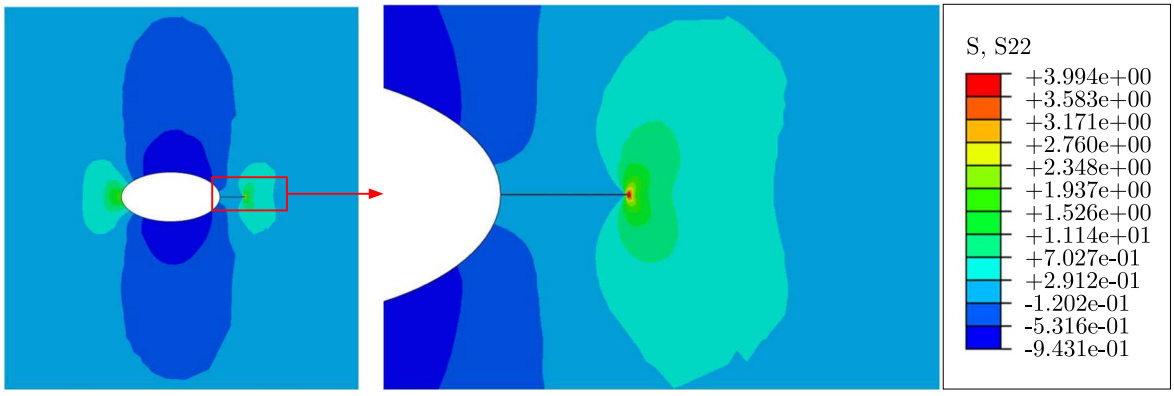

Fig. 8. σ_{yy} force cloud diagram

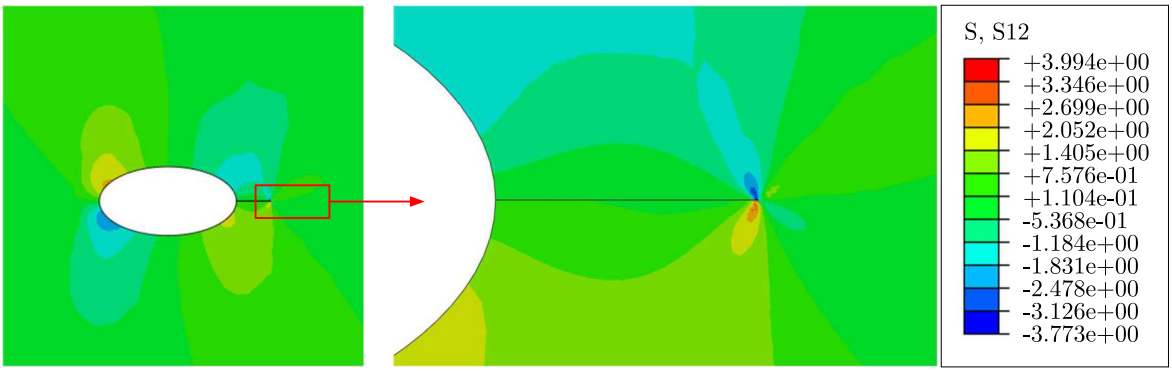

Fig. 9. τ_{xy} force cloud diagram

3.3. Analysis of factors influencing the crack tip intensity factor

To further explore the variation law of the stress intensity factor at the crack tip, it is calculated based on different lengths of elliptical hole edge cracks and elliptical hole flatness. For ease of calculation, the crack length and elliptical hole parameters are taken as dimensionless values. Figure 10 shows a comparison between the analytical and simulated solution of the stress intensity factor at the crack tip in function of crack length for elliptical holes $a = 2$, $b = 1$ and $q = 1$. As shown in the figure, as the crack length increases and the stress intensity factor error gradually decreases. The maximum error of the stress intensity factor shall not exceed 3%. This proves the correctness of the stress intensity factor for a single hole stress in this paper.

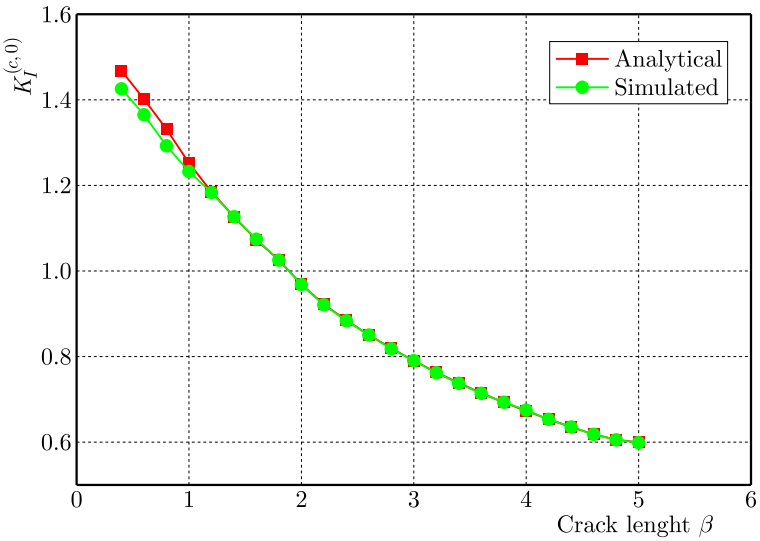

Fig. 10. Comparison of analytical and simulated solutions for stress intensity factor changes with crack length at $a = 2$ and $b = 1$

As illustrated in Fig. 11, by controlling the parameter b of the elliptical hole, while maintaining $c = 1$, $a = 1$ and $q = 1$, the calculated analytical solution is compared with the simulated solution. As shown in the figure, when the value of b increases, the stress intensity factor first increases slowly and does not change much. It reaches its maximum value when the value of b reaches about 0.55, and then rapidly decreases to a parabolic shape. Furthermore, when b approaches 0, the problem of elliptical holes with cracks degenerates into a classical problem of partial stress inside the crack. After calculation, the stress intensity factor at the tip is 0.677, which is consistent with the classical results in reference (Li *et al.*, 2010). The same conclusion can be drawn when the internal part of the crack is subjected to force.

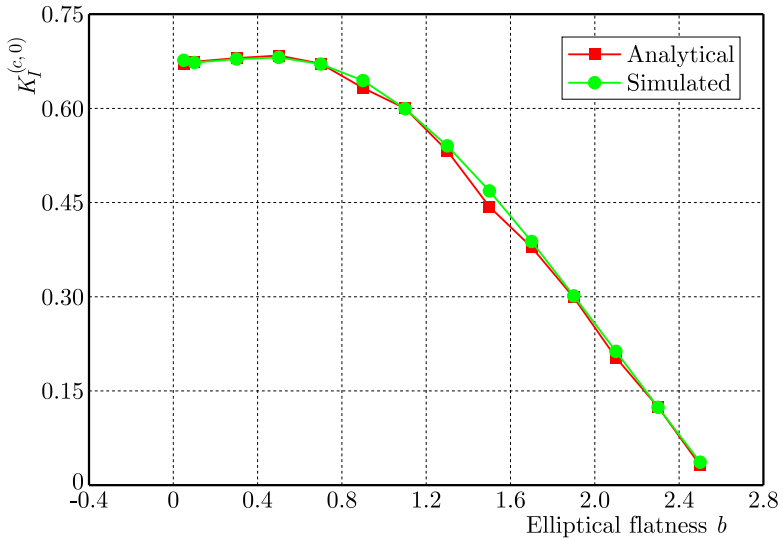

Fig. 11. Comparison of analytical and simulated solutions for a change in the crack tip intensity factor with elliptical flatness at $a = 1$, $\beta = 1$

When $a = b$, the problem of elliptical holes with cracks degenerates into a problem where a single circular hole is subjected to a force while the crack surface is not subjected to the force. A more extensive analysis of this issue is provided in this article. Figure 12 shows a comparison between the analytical and simulated solution of the stress intensity factor at the crack tip in function of the radius of the circular hole when the crack length $\beta = 1$ and $q = 1$. As shown in Fig. 12, when the radius of the circular hole increases, the rate of change of the stress intensity factor at the crack tip increases first and then decreases.

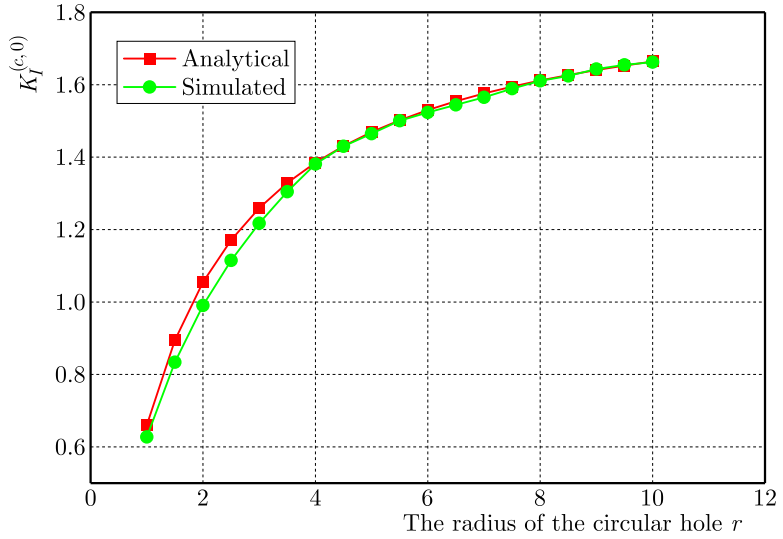

Fig. 12. Change of the stress intensity factor at the crack tips for different lengths with r at $\beta = 1$

Figure 13 shows a comparison between analytical and simulated solutions for variation patterns of the stress intensity factors under different conditions calculated using the method presented in this paper. As can be seen from Fig. 13, when the crack length changes, the stress intensity factor first increases rapidly to the peak and then slowly decreases. When a/β is about 0.5, the stress intensity factor reaches its peak.

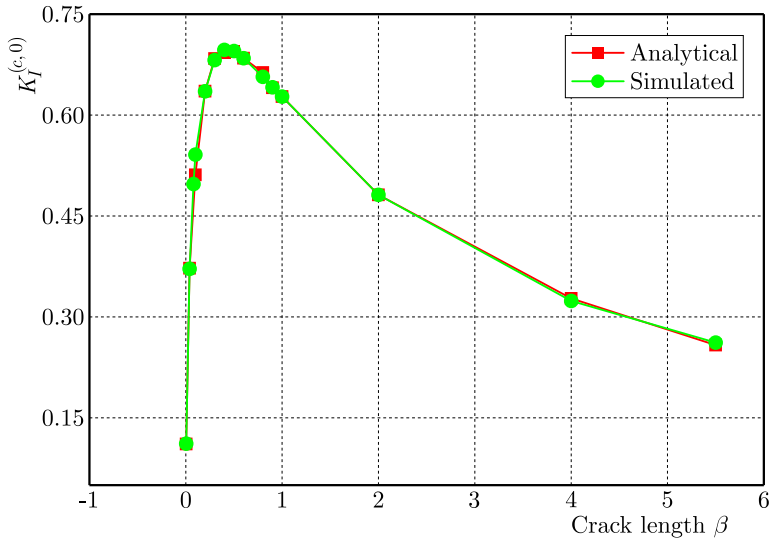

Fig. 13. Comparison of the analytical and simulated solutions for the stress intensity factor at the crack endpoint and crack length change at $a = 1$ and $b = 1$

4. Conclusion

- A transcendental function has been constructed using the Muskhelishvili method and number theory to solve the complex problem of elliptical holes with cracks. The analytical solution to the stress intensity factor at the crack tip has been obtained, which is a further extension of the Muskhelishvili complex function method and expands its application range.
- Verification based on an Abaqus numerical simulation method has been made, and the results showed that after the elliptical hole was loaded, the stress concentration area appeared near the crack tip. By comparing the analytical solution of the stress intensity factor at the crack tip with the corresponding simulated solution, the correctness of the analytical solution for a single hole under stress was confirmed.
- Further analysis was carried out on the influencing factors of the crack tip strength factor (elliptical hole edge crack length, elliptical hole flatness, circular hole radius): (1) when $a \neq b$, with the increase of short radius b, the stress intensity factor first slowly increases and does not change much, reaching its maximum value when b reaches around 0.55, and then rapidly decreases in a parabolic shape; (2) when $a = b$, as the radius of the circular hole increases, the rate of change of the stress intensity factor at the crack tip first increases and then decreases. When $a = b = 1$, the crack length changes, and the stress intensity factor first rapidly increases to the peak, then slowly decreases.

Acknowledgements

This research was supported by the National Natural Science Foundation of China (Grant No. 52074167) and the Natural Science Foundation of Shandong Province (Grant No. ZR2020QE135). The authors of this article are very grateful for the support provided.

References

1. Alderliesten R.C., 2007, On the available relevant approaches for fatigue crack propagation prediction in GLARE, *International Journal of Fatigue*, **29**, 2, 289-304

2. Aliabadi M.H., Rooke D.P., Cartwright D.J., 1987, An improved boundary element formulation for calculating stress intensity factors: Application to aerospace structures, *The Journal of Strain Analysis for Engineering Design*, **22**, 4, 203-207

3. Andrasic C.P., Parker A.P., 1984, Dimensionless stress intensity factors for cracked thick cylinders under polynomial crack face loadings, *Engineering Fracture Mechanics*, **19**, 1, 187-193

4. Bakuckas J.G., 2001, Comparison of boundary correction factor solutions for two symmetric cracks in a straight-shank hole, *Engineering Fracture Mechanics*, **68**, 9, 1095-1106

5. Bowie O.L., 1956, Analysis of an infinite plate containing radial cracks originating at the boundary of an internal cirular hole, *Journal of Mathematics and Physics*, **35**, 60

6. Bowie O.L., 1964, Rectangular tensile sheet with symmetric edge cracks, *Journal of Applied Mechanics*, **31**, 2, 208-212

7. Brennan F.P., Teh L.S., 2004, Determination of crack-tip stress intensity factors in complex geometries by the composition of constituent weight function solutions, *Fatigue and Fracture of Engineering Materials and Structures*, **27**, 1

8. Chen F., Sun Z., Xu J., 2001, Mode I fracture analysis of the double edge cracked Brazilian disk using a weight function method, *International Journal of Rock Mechanics and Mining Sciences*, **38**, 3, 475-479

9. Deng P., Matsumoto T., 2017, Weight function determinations for shear cracks in reinforced concrete beams based on finite element method, *Engineering Fracture Mechanics*, **177**, 61-78

10. Fett T., 1992, Direct determination of weight functions from reference loading cases and geometrical conditions, *Engineering Fracture Mechanics*, **42**, 3, 435-444

11. Gao C.F., Kessler H., Balke H., 2003a, Crack problems in magnetoelectroelastic solids. Part I: Exact solution of a crack, *International Journal of Engineering Science*, **41**, 9, 969-981

12. Gao C.F., Kessler H., Balke H., 2003b, Crack problems in magnetoelectroelastic solids. Part II: General solution of collinear cracks, *International Journal of Engineering Science*, **41**, 9, 983-994

13. Guo T., Qu Z., Gong F., Wang X., 2017, Numerical simulation of hydraulic fracture propagation guided by single radial boreholes, *Energies*, **10**, 10, 1680-1692

14. Hasebe N., Chen Y.Z., 1996, Stress intensity solutions for the interaction between a hole edge crack and a line crack, *International Journal of Fracture*, **77**, 351-366

15. Li S., He T., Yin X., *et al.*, 2010, *The Introduction of Rock Fracture Mechanics* (in Chinese), Hefei: University of Science and Technology of China Press

16. Parker A.P., Andrasic C.P., 1983, On the determination of stress intensity factors for cracked thick cylinders, *MRS Online Proceedings Library (OPL)*, **22**, 1, 227

17. Xu W., Wu X.R., Yu Y., Li Z.H., 2018, A weight function method for mixed modes hole-edge cracks, *Fatigue and Fracture of Engineering Materials and Structures*, **41**, 1, 223-234

18. Xu Y., Yang J., 2022, Anti-plane fracture problem of a regular hexagonal hole with radial edge cracks in piezoelectric/piezomagnetic composites (in Chinese), *Chinese Quarterly Of Mechanics*, **43**, 1, 149-158

19. Yan X., 2007, Rectangular tensile sheet with single edge crack or edge half-circular-hole crack, *Engineering Failure Analysis*, **14**, 7, 1406-1410

20. Zhang W., Guo W.Y., Wang Z.Q., 2022, Influence of lateral pressure on mechanical behavior of different rock types under biaxial compression, *Journal of Central South University*, **29**, 11, 3695-3705

21. Zhang W., Zhang B.L., Zhao T.B., 2023a, Study on the law of failure acoustic-thermal signal of weakly cemented fractured rock with diferent dip angles, *Rock Mechanics and Rock Engineering*, **56**, 6, 4557-4568

22. Zhang W., Zhao T.B., Zhang X.T., 2023b, Stability analysis and deformation control method of swelling soft rock roadway adjacent to chambers, *Geomechanics and Geophysics for Geo-Energy and Geo-Resources*, **9**, 1, 91

23. Zhao J., Xie L., Liu J., Zhao Q., 2012, A method for stress intensity factor calculation of infinite plate containing multiple hole-edge cracks, *International Journal of Fatigue*, **35**, 1, 2-9

24. Zhou J., Wang G., Li L., *et al.*, 2020, Truncated conformal mapping approach for four cracks with unequal length emanating from elliptical hole-edge in infinite plates (in Chinese), *Journal of Inner Mongolia Normal University (Natural Science Edition)*, **49**, 1, 35-38

25. Zhu Q., Han F., Sui M., 2016, Stress intensity factors and crack-surface opening displacements for two cracks emanating from a circular hole in an infinite plate, *Acta Aeronautica et Astronautica Sinica*, **37**, 3, 883-893

Manuscript received July 11, 2023; accepted for print December 1, 2023